Annu. Rev. Phys. Chem. 2000. 51:623–53

THEORETICAL STUDIES OF ATOMIC-SCALE PROCESSES RELEVANT TO CRYSTAL GROWTH

Hannes Jónsson
Department of Chemistry 351700, University of Washington, Seattle, Washington 98195-1700; e-mail: hannes@u.washington.edu

Key Words pattern formation, adsorption, diffusion, transition states, surface dynamics

■ **Abstract** The study of adsorption, diffusion, island formation, and interlayer transport of atoms on a growing surface has been an active field in the past decade, because of both experimental and theoretical advances. Experiments can give detailed images of patterns formed on growing surfaces. An important challenge to the theoretical studies is the identification of dynamical processes controlling the pattern formation and overall surface morphology. This can be achieved by accurate modeling of the atomic interactions, a thorough search for active atomic-scale processes, and simulation of the growth on the experimental timescale to allow for detailed comparison with the experimental measurements. An overview of some of the theoretical methodology used in these studies and results obtained for one of the most extensively studied systems, Pt(111), is given here. A remarkable richness of phenomena has emerged from these studies, where apparently small effects can shift the balance between competing molecular processes and thereby change the morphology of a growing surface. The article concludes with a discussion of possible future directions in this research area.

INTRODUCTION

Crystal growth is intriguing in many ways. The process of transformation from a disordered phase (gas or liquid) to a highly ordered arrangement of atoms in a nearly perfect crystal is a remarkable one. The study of crystal growth kinetics at the atomic scale is a study of the shape of the free-energy surface that in one way or another causes the atoms to give up their random translational motion and congregate to form various patterns, eventually resulting in a highly ordered, crystalline solid. One can make the same arguments here as did Levinthal in his famous "paradox" on protein folding (1); the number of different arrangements the atoms can take is staggering. If every one had to be tried at random, the timescale of the ordering process would be much too long. In crystal growth, the guiding principles appear to be clearer than in protein folding: Atoms get attracted to steps and from there get attracted to kinks, which are the natural growth sites. But this simple

0066-426X/00/1001-0623$14.00

scenario only holds in the simplest growth regime, the step flow. As is illustrated below, the pathways are more complex and subtle farther away from equilibrium, where new islands form on the flat terrace and a delicate balance between competing processes determines the shape of the islands, which can, in turn, determine the large scale morphology of the growing surface (smooth vs rough).

The fast progress in atomic-scale crystal growth studies in the past decade has been driven to large extent by the emergence of powerful tools for imaging surfaces at the atomic scale, mostly by scanning tunneling microscopy (STM) (2). Scattering experiments using He atoms (3) and electrons (4, 4a) have also given valuable information about the surface morphology during growth. Field ion microscopy (FIM) experiments have also given valuable information about surface diffusion. An important role of theoretical studies has been the identification of the atomic-scale processes that give rise to the experimentally observed surface structure. Ultimately, one would like to answer a number of questions. For example, does the surface of the growing crystal remain smooth or does it become rough? For what conditions is an amorphous solid rather than a crystal obtained? Some materials technology is based on growing thin crystalline films on substrates at as low a temperature as possible to prevent interdiffusion. Effective control of the growth morphology relies on choosing conditions and systems that shift the balance between competing atomic-scale processes in such a way as to favor the desired outcome. A theoretical prediction of the growth process requires accurate description of the atomic interactions and analysis of the rates of various atomic-scale transitions, and eventually a simulation of the growth on the timescale of the experiments. This problem is harder than it may seem.

The interaction of atoms can be described at various levels of theory. The most generally applicable approach is the first principles, or ab initio approach (5), where no adjustment of parameters is made to fit information about chemical bonds. A typical error bar is quoted as ± 0.1 eV in such calculations, but higher accuracy is needed to be able to predict thermally activated dynamics at a typical temperature.

Once the atomic interactions have been described, the hardest problem in theoretical crystal growth studies is the identification of the important atomic-scale processes. What kinds of processes are important, and what is the mechanism? At first sight, it might seem that numerical simulations of the classical dynamics, i.e. finite difference solution of Newton's equation of motion, would be a relatively straightforward way of reproducing the laboratory experiments, and one could simply observe the processes occuring in the simulation. Such classical dynamics simulations of atoms and molecules have led to valuable insight and improved understanding of atomic-scale processes in many diverse areas of science (6). But direct classical dynamics simulations are limited to very short timescales, even when simple empirical potential functions are used to describe the atomic interactions, about a nanosecond of real time for a week of computations. This represents a severe limitation on the types of phenomena that can be studied. Important crystal growth processes such as diffusion and conformational changes of

islands are typically "rare events," in that the atoms vibrate about their optimal position multiple times in between these events. For example, the activation energy for the diffusion of a Pt adatom along the edge of a Pt step (7) is ca 0.7 eV, and the diffusion of a Si adatom on top of the Si(100) surface (8) is ca 0.6 eV. Such a diffusion event occurs several times per second at room temperature and is active on the laboratory timescale. But there are on the order of 10^{10} vibrational periods in between diffusion events. A direct classical dynamics simulation that necessarily has to faithfully track all this vibrational motion would take on the order of 10^5 years of computer calculations on the fastest present-day computer before a single diffusion event can be expected to occur. It is clear that meaningful crystal growth simulations cannot be carried out for typical systems by simply simulating the classical dynamics of the atoms. It is essential to carry out the simulations on a much longer timescale. This timescale problem is one of the most important challenges in computational chemistry, materials science, and condensed-matter physics.

If all the important processes that can occur in the system have been identified, it is relatively straightforward to estimate the rates and simulate the crystal growth process, as is explained below. The most challenging part is to identify relevant processes that are slow on the vibrational timescale. Recently, new methods for approaching this problem systematically have been proposed, but so far intuition and serendipity or a combination of the two have been used (see below). Many surprising processes have been found and more will likely be found in the future.

This review article focuses on one particular system that has received a great deal of attention in the past decade, the growth of Pt(111). This is probably the most extensively studied crystal growth problem. The atomic-scale mechanisms of island formation and growth are discussed in some detail, especially results that are unexpected or even counterintuitive. To limit the length of this review, the discussion necessarily omits many interesting and important studies. The choice of system discussed here simply reflects my own personal preference and thereby also includes many studies that I and my research group have been involved in.

The growth of the (111) surface of a Pt crystal is an example of homoepitaxial growth. Technologically, the growth of a crystal on top of a different type of crystal, i.e. heteroepitaxy, is more important, but also more complex. Issues such as mixing, surface alloying, and strain-dominated processes need to be dealt with, in addition to the issues present in homoepitaxial growth. Much less theoretical work has been done on these more complex systems, but a great deal of experimental effort is currently being devoted to this area, for example metal films on metaloxides (9), ice grown on metal substrates (10, 10a), and multilayer semiconductor films (11). Heteroepitaxy will likely be a major focus of future crystal growth studies.

This review first focuses on the theoretical methodology relevant to crystal growth studies, followed by an application to Pt(111) growth. The article concludes with a discussion of future directions.

METHODS

Before discussing particular crystal growth processes, a brief overview is given of some of the methods that have proven to be useful in the past. Also, promising new methods are mentioned.

Interatomic Interactions

The forces acting between the atoms have in almost all cases been calculated within the Born-Oppenheimer (adiabatic) approximation, i.e. it is assumed the atoms are moving on the ground-state potential energy surface. Estimates of electron-hole pair coupling to the atomic dynamics have been made and in some cases small but significant contributions are suggested (12, 12a). Nonadiabatic effects are necessarily involved in some instances, for example the adsorption of a Si atom on a Si surface, where the triplet ground state of the incoming atom gets converted to a singlet state.

First Principles Methods The phrase first principles is used here to mean a method where measurements of chemical bonds have not been used for parametrization.

Very rapid advance has been made in the past 10 years in the application of density functional theory (DFT) (5, 13, 13a) to study the energetics of condensed-phase dynamics, in particular surface diffusion (see for example 14–15b). The method of choice for surface calculations is simulation of a slab where periodic boundary conditions are enforced parallel to the surface. A plain wave basis set is used in combination with pseudopotentials (19, 20). This field has advanced to the point that calculations of structures and stable configurations are routine. A researcher wishing to carry out such calculations can choose from different software packages, including VASP (16, 16a) and DACAPO (17), which are highly optimized and yet written in such a way as to make the calculations relatively easy. The calculation of transition states and dynamics are less routine but have also advanced greatly.

DFT calculations of surface dynamics have been very successful. In some cases, they have led to reinterpretation of experimental data (14, 18). Examples for Pt(111) are given below. It is important to keep in mind, though, that the DFT calculations are not exact, mainly because the true density functional is not known. A calculation of the relative energy of two configurations is typically considered to have an error bar of 0.1 eV if the configurations are similar. These estimates rely on cancellation of errors. The situation is worse when the configurations being compared differ significantly and can be better if they are very similar. Furthermore, the small size of the systems can make it impossible to include long-range elastic strain effects properly. This can easily lead to errors on the order of 0.1 eV (18). This accuracy is sufficient to learn about the important features of the potential energy surface, to determine which processes are likely to be important,

and what the overall mechanism is. However, thermal energy at room temperature, for example, is only 0.025 eV, so significantly higher accuracy is needed before potential surfaces calculated by DFT can be expected to reproduce experimental measurements without some modifications. DFT calculations of much larger systems (several hundred atoms) are becoming doable with linear scaling algorithms (21–21b) and faster computers. It is, however, less clear whether the basic approximations in the density functionals can be improved easily to get much higher accuracy.

Several different functionals are currently being used (22–24), but the PW91 functional is closest to being the current "standard" in surface-dynamics simulations (24). Detailed comparison of various functionals, as well as comparison with more traditional first-principles calculations, has, for example, been carried out for Si adatom binding and diffusion on a Si(100) surface (25). It was found that PW91 gives significant improvement over local density approximations (LDA), and the results agreed quite well with QCISD(T) (26) calculations when applied to clusters. The BLYP functional, which is used more often in calculations of molecules (5), was found to do less well for Si clusters. Also, comparison of DFT calculations with detailed STM measurements of Si addimer rotation on Si(100) indicated that the BLYP is less accurate for Si than is PW91 (27). This situation is different for some other systems. For example, the desorption of H_2 from Si(100) surface modeled with high-level calculations on a small cluster was significantly better represented by the BLYP functional than by PW91 (28). At this stage, it is important to test the applicability of DFT and the various functionals for each new system, using small clusters as test models for which high-level wave function–based calculations [such as QCISD(T)] can be applied.

It seems evident that careful comparison of theoretical results with experimental measurements of surface dynamics will remain essential in the foreseeable future to refine energy surfaces obtained by first-principles approaches.

Empirical Potentials Another approach to the evaluation of interatomic forces is the construction of empirical or semiempirical potential energy functions. A great deal of work has been done on modeling metals, including the effective medium theory (EMT) (29, 29a) and embedded atom method (EAM) (30–31) approaches, as well as semiconductors, in particular Si (32–32b). When successful, this enables the simulation of much larger systems and much more thorough exploration of the potential energy surface to search for relevant processes. Covalent and metal bond breaking and bond forming processes have, however, proven to be hard to mimic accurately enough with empirical potentials. A great deal of work, insight, and ingenuity has gone into constructing such potential energy surfaces, and many properties can be reproduced accurately, but these potential functions are typically tailored to bulk properties and the description of the dynamics of adatoms on a surface is typically outside the range of validity. Although the surface diffusion on some metal surfaces is well described by such potential functions, there are also systems, in particular Pt, where this approach can at best be considered to

give a rough, qualitative estimate (33). Significant quantitative (and even qualitative) differences between the results of these approaches and DFT results have been found (18, 34). Some examples are given below, however, where studies of Pt crystal growth processes using empirical potentials have led to valuable insight and identification of phenomena that have later proved to be consistent with DFT calculations. The situation is worse for covalent materials, such as Si. This is a much more difficult system to mimic with a potential function. The various different hybridizations of Si and delocalized (both sigma and pi) as well as localized bonding are difficult to capture in a potential function to high enough accuracy. The energy landscape for the diffusion of a Si adatom on a Si surface given by the empirical potentials is very different from the DFT results (25). Molecular systems, such as ice, may hold a greater promise for empirical potential functions because the interaction is largely electrostatic and can therefore be modeled rigorously (35–35b). It is essential for ice surface studies to go beyond simple pairwise potentials and include environment dependence, for example induced dipole due to local electric field. In ice, the molecular dipole moment is predicted to be 3.1 D within the induction model, whereas it is 2.6 D at the surface and only 1.85 D in the gas phase (35–35b). This environment dependence can have significant effect on the energetics and rates of crystal growth processes.

Identifying Relevant Processes and Locating Transition States

The timescale problem mentioned above is devastating for direct dynamical simulations but makes it possible to get accurate estimates of transition rates by using purely statistical methods, namely transition state theory (TST) (36–40). Apart from the Born-Oppenheimer approximation, TST relies on two basic assumptions: (*a*) The rate is slow enough that a Boltzmann distribution is established and maintained in the reactant state, and (*b*) a dividing surface of dimensionality $3N - 1$ where N is the number of atoms in the system can be identified and it is assumed that a reacting trajectory going from the initial state to the final state only crosses the dividing surface once. The dividing surface must, therefore, represent a bottleneck for the transition. The TST expression for the rate constant can be written as

$$k = \frac{\langle |v| \rangle}{2} \frac{Q^{\ddagger}}{Q_R},$$

where $\langle |v| \rangle$ is the average speed, $Q^{\ddagger}$ is the configuration integral for the transition state dividing surface, and Q_R is the configuration integral for the initial state. The bottleneck can be of purely entropic origin, but most often in crystal growth problems it is due to a potential energy barrier between the two local minima representing the initial and final states. It can be shown that TST always overestimates the rate of escape from a given initial state (37) [a diffusion constant can be underestimated if multiple hops are not included in the analysis (38)]. This leads to a variational principle that can be used to find the optimal dividing surface (37, 39).

TST does not say anything about the final state of the transition. The possible final states can be determined by short time simulations of the dynamics starting from the dividing surface. This can also give an estimate of the correction to TST due to recrossing of the dividing surface, the so-called dynamical corrections (40).

The variational optimization of the transition state dividing surface for the purpose of obtaining an optimal estimate of the rate constant can, therefore, also be a search for the most important transition mechanism. In a recent formulation of TST, so-called optimal hyperplanar TST (OH-TST), a hyperplanar dividing surface is moved gradually from the initial state toward an assumed final state while the orientation as well as location of the hyperplane is optimized until both the translational and rotational force acting on the plane have been zeroed (41). This method is an extension of a previous formulation where the orientation of the hyperplane was not optimized but was some predefined function of the location (42). The free energy barrier is evaluated from the reversible work of translating and rotating the plane. Although the motion of the hyperplane is typically started by assuming some final state, the optimized hyperplanar dividing surface may end up being a transition state corresponding to a different, unexpected mechanism. This has been illustrated by an example from Al adatom diffusion. Feibelman predicted from DFT calculations that an exchange process involving the adatom and a surface atom is the optimal diffusion mechanism rather than the more straightforward hop mechanism (43). In a OH-TST calculation using an EAM potential where a hyperplane is initially moved gradually toward the final state of a hop, the converged optimal transition state was found to be that for an exchange process (41). Note that the final state of the exchange process is different from the hop, and this was utilized by Kellogg & Feibelman (44) to determine that the diffusion of a Pt adatom on a Pt(100) surface does, in fact, occur by the exchange mechanism. This example demonstrates the importance of being able to search for the mechanism of a transition without strong bias from a preconceived notion. Many surprising mechanisms have emerged from studies of surface dynamics in the past decade.

Because atoms in crystals are usually fairly tightly packed and the relevant temperatures are low compared with the melting temperature, the harmonic approximation to TST (hTST) can typically be used in studies of crystal growth without much loss of accuracy (40). This greatly simplifies the problem of estimating the rates. The search for the optimal transition state then becomes a search for the lowest few saddle points at the edge of the potential energy basin corresponding to the initial state. The rate constant for transition through the region around each one of the saddle points can be obtained from the energy and frequency of normal modes at the saddle point and the initial state (45, 45a)

$$k^{\mathrm{hTST}} = \frac{\prod_i^{3N} \nu_i^{\mathrm{init}}}{\prod_i^{3N-1} \nu_i^{\ddagger}} e^{-(E^{\ddagger} - E^{\mathrm{init}})/k_B T}.$$

Here, $E^{\ddagger}$ is the energy of the saddle point, E^{init} is the local potential energy minimum corresponding to the initial state, and the ν_i are the corresponding normal

mode frequencies. The symbol ‡ refers to the saddle point. The most challenging part in this calculation is the search for the relevant saddle points. Again, the mechanism of the transition is reflected in the saddle point. The reaction coordinate at the saddle point is the direction of the unstable mode (the normal mode with negative eigenvalue). After a saddle point has been found, one can follow the saddle point along the unstable mode, both forward and backward, and map out the minimum energy path (MEP), thereby establishing what initial and final state the saddle point corresponds to. The identification of saddle points ends up being one of the most challenging tasks in theoretical crystal growth studies.

It is also important to estimate the prefactors. Various diffusion rates that have been determined experimentally tend to have similar prefactors (46). This corresponds to a preexponential of roughly 10^{12} sec^{-1} in the hTST expression of the rate constant given above. Often this or a close number is simply assumed to be the appropriate prefactor for all the surface processes instead of going through the evaluation of all the normal mode frequencies. However, prefactors for two competing processes can easily differ by one or two orders of magnitude, and this can lead to crossover from one mechanism to another as temperature is varied (see for example 47). A two-orders-of-magnitude variation in a prefactor changes the rate at room temperature by as much as a 0.1-eV adjustment of the activation energy, a typical error bar in a DFT calculation.

The NEB Method When the initial and final state of a transition is known, a robust method can be used to find the MEP and thereby the saddle point, which is the point of maximum energy along the MEP. Initially, a string of replicas of the system is generated using some interpolation between the initial and final state of the transition (usually a linear interpolation). The replicas are connected with springs so as to guarantee a continuous path (see Figure 1*a*). Then an optimization algorithm involving force projections is used to relax the replicas toward the MEP (42,48,49). If the same spring constant is used for all the replicas, the method results in an even spacing of the images along the MEP. It can be useful to vary the spring constant so as to increase the density of images in the more important saddle point region. Although the saddle point is the only important point for the harmonic TST rate estimate, in addition to the initial point, the MEP gives a useful, extended view of the potential energy landscape. For example, the optimal transition mechanism may involve a more complex path with one or more intermediate minima. This was, for example, observed in calculations of descent of Pt atoms at kink sites on the Pt (111) surface (50). Although a linear interpolation was used as a starting configuration of the replicas, the converged nudged elastic band (NEB) showed an optimal mechanism that involved two hops of the adatom on the upper terrace before descending to the lower terrace, a final path that is very different from the initial linear interpolation. Also, it sometimes happens that the MEP has intermediate minima that are lower in energy than the initial state (51). This nonlocal view of the most relevant part of the potential energy landscape is not obtained from a method that simply converges to the nearest saddle point.

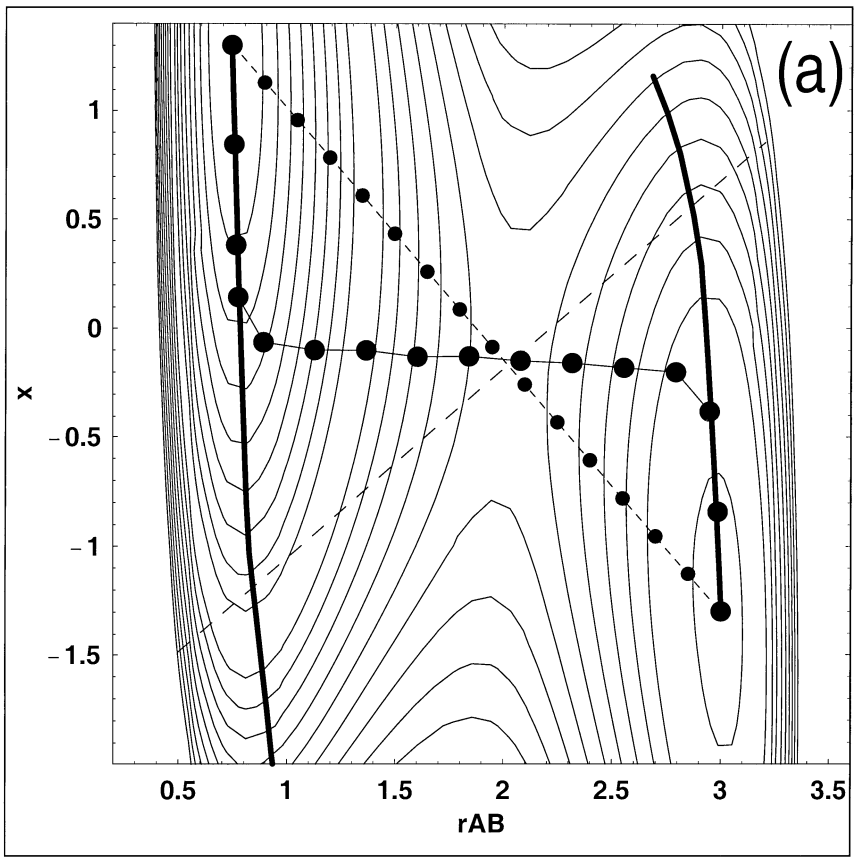

Figure 1 Methods for calculating the activation energy for transitions. (*a*) The NEB method for finding minimum energy paths (MEPs) and saddle points. (*Small, filled circles*) The initial configuration of replicas of the system. A spring force acts between adjacent replicas and regulates the separation between them. After the optimization, which involves force projections of both the true forces and the spring forces, the replicas line up on the MEP (*larger, filled circles*). A "drag" procedure where one coordinate, the "drag coordinate" (here chosen to be the *line* from initial state to final state), is fixed while all other degrees of freedom are relaxed, leads to the *solid lines*. Here the system follows the slowest ascent paths, which do not lead to the saddle point. Even when the drag coordinate coincides with the saddle point, the relaxation in the orthogonal coordinates (*dashed line*) allows the system to fall down from the saddle point region into the potential valley on either side. (See Reference 48.) (*b*) The dimer method for finding saddle points. Two replicas of the system are formed and kept at a fixed separation from each other. At each point, the dimer is rotated to minimize the energy. The minimum energy direction gives the lowest-frequency normal mode. The component of the force, $\vec{F}_R$, in the direction of the dimer is then reversed to give an effective force, $\vec{F}^{\dagger}$, which drives the dimer to the saddle point. This method can be used to climb up the potential surface and search for saddle points, or to refine the estimate obtained from the NEB method. (From Reference 55.)

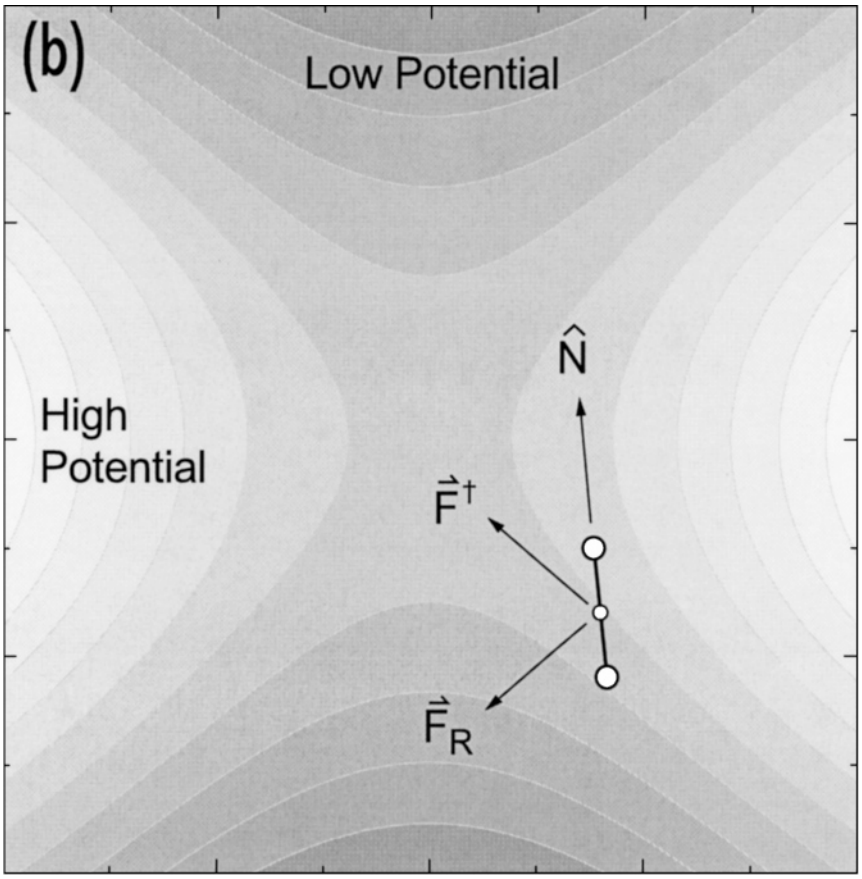

Figure 1 (*Continued*)

The Dimer Method Most often, only the initial state of a transition is known, and both the final state and the mechanism of the transition are unknown. Then a climb up the potential surface starting from the initial local minimum and converging on a saddle point is needed. This can be done with so-called eigenvector-following methods, which are commonly used in studies of molecules and small clusters (52–54). Here, the Hessian matrix of second derivatives is constructed and then diagonalized to get the eigenvectors at each point along the climb. But crystal growth studies employing empirical potentials typically involve many atoms, on the order of several hundred to several thousand, making eigenvector following unpractical because of the N^3 scaling. DFT calculations necessarily involve much smaller systems, on the order of 50–100, but ideally they make use of plane waves as basis functions to eliminate boundary effects and thereby cannot produce estimates of the second derivatives unless a great deal of computer time is involved.

Recently, a new method has been presented requiring only first derivatives of the energy while maintaining the essential qualities of the eigenvector-following method (55). The method involves construction of two replicas of the system, a dimer, as illustrated in Figure 1*b*. The dimer is rotated about its center in order to find the direction of the lowest frequency mode, and then the component of the force acting on the center of the dimer is reversed along the direction of the dimer. Any optimization algorithm that moves the dimer according to this modified force will then converge on the saddle point. The method is called the dimer method, and it has been applied to the study of the diffusion mechanism of an Al adatom on an Al(100) surface (55). A swarm of these searches were started up at random near the local minimum corresponding to the initial state. In addition to the hop and two-atom exchange processes, four-atom and three-atom exchange processes were also found, with almost equally low saddle points as the hop. At higher energy, a large number of processes were observed, some involving formation of local reconstruction of the surface. This method seems to be promising for identifying the mechanism of transitions when the final state is not known. It is also a fast way of homing in on the saddle point once a rough estimate has been obtained. When a final state is known, it is likely that an optimal approach is to start with a few iteration of the NEB, to see what the energy landscape looks like, and then converge on the saddle point by using the dimer method with a starting point obtained by interpolation of the partially relaxed NEB chain.

Accelerated Dynamics Recently, Voter proposed a method for accelerating classical dynamics simulations, which can, in particular, be applied to crystal growth processes (56–56b). The method, called hyperdynamics, involves constructing a repulsive bias potential, which effectively reduces the activation energy of the transition, thereby increasing the transition rate. In order for this kind of approach to be effective in multidimensional systems, it is important to construct the bias potential in a nontrivial way, as explained by Voter. The true timescale can be related to the simulation by using transition state theory. In that sense, the simulation is statistical in nature; the dynamics are only used to search the configuration space. Such a statistical sampling can be carried out with multiple simulations in parallel, further increasing the timescale that can be simulated (56). This methodology has recently been applied to simulations of Cu(100) growth, spanning a timescale of several seconds (57). Unexpected processes involving concerted motion of several atoms were observed in these simulations.

Another approach is to use elevated temperature to speed up the simulated dynamics. This has been used in crystal growth simulations, but the problem is that entropic effects can lead to crossover to a different mechanism as the temperature is increased. Basically, entropic effects will dominate over energy at high enough temperature, thereby favoring a different transition mechanism. A better approach is to use the elevated dynamics only as a way to search for final states and then use a NEB calculation, for example, to identify the saddle point for each transition identified by the simulations. Harmonic TST can then be used to estimate the rate

at the low temperature of interest. This approach was used by Sørensen et al (58) in studies of the deformation of a nanoscale metal tip brought up to a metal surface. With this method, it could be estimated at which distance thermally activated processes would lead to contact formation given the timescale and temperature of the experiment. Sørensen & Voter (59, 59a) have developed an algorithm where an estimate of the required simulation time at the elevated temperature is inferred from an assumed lower bound on the prefactor. Their algorithm also involves a reflection of the simulated trajectory from a dividing surface each time a transition is detected.

A third approach is to use a method to climb up the surface and find all relevant saddle points for a given initial state, for example by using the dimer method (55). Long timescale dynamics within harmonic TST would involve a search of saddle points for transitions from a given configuration. A random number can then be used to choose between the different transitions corresponding to the various saddle points in proportion to the relative rates. The system then gets advanced to the final state of the transition, and again a search for saddle points is carried out, etc. In the analysis of the Al adatom diffusion (55), the four lowest-energy saddle points for diffusion were found in 75% of the runs, indicating that it would be sufficient to carry out a few tens of runs, with a total of less than 10,000 force evaluations to find the mechanism and rate of the next transition. This kind of algorithm maps well on a cluster of computers. An independent search for a saddle point can be carried out on each computer.

Kinetic Monte Carlo Simulations

If all relevant processes in the system have been identified, and the rate of each process has been estimated, the time evolution of the system can be described by a set of coupled rate equations that can be solved by using random numbers (60–63). This is the so-called kinetic Monte Carlo (kMC), or time-dependent Monte Carlo procedure. The problem here is that one can never be sure that all relevant processes have been identified. The quality of the simulation is only as good as the quality of the input. Erroneous results will be obtained if an important process is missing.

It is necessary to come up with some classification scheme of the various active processes. Voter has discussed the case of FCC(100) surfaces (64, 64a). On FCC(111) surfaces, the interactions have a longer range (because the surface is less corrugated), and it is necessary not only to specify the number of neighbors in the initial and final state, but also the coordination of the neighbors. An undercoordinated neighbor can relax more than a highly coordinated neighbor. A classification scheme for a FCC(111) surface is illustrated in Figure 2 (65). Here the coordination number of various neighboring atoms is specified and an example of a list of a few possible transitions is given in Table 1, with reference to Figure 2*b*. Clearly, the number of entries in the table becomes unmanageable unless some wild cards are used, but it is important to be able to distinguish between the two

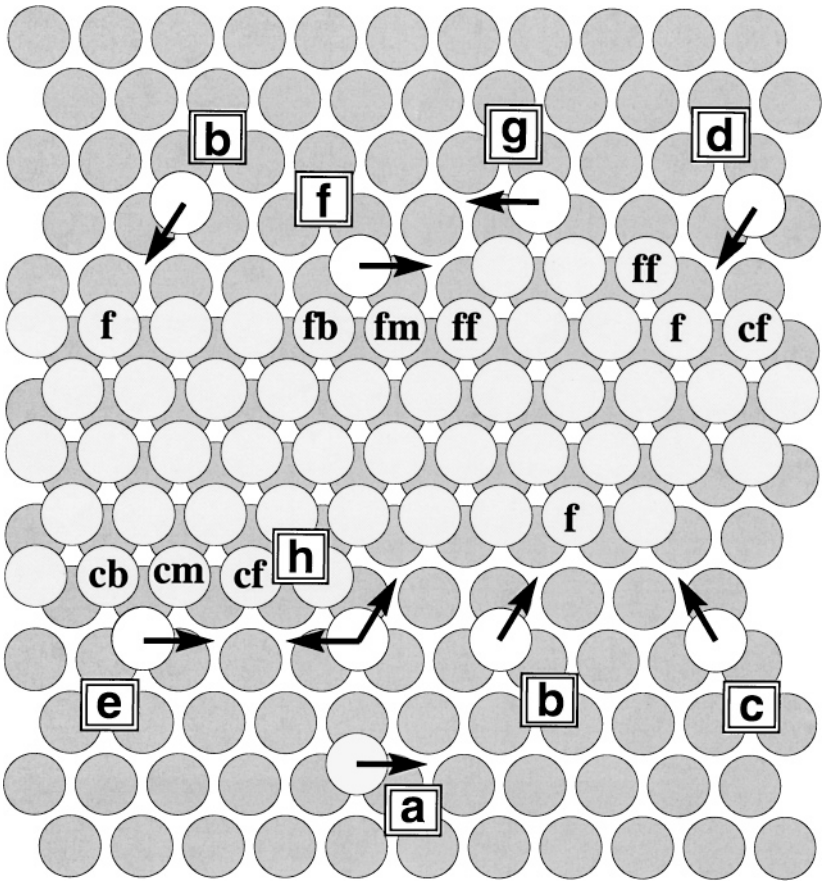

Figure 2 Some examples of diffusion hops on the FCC(111) surface. The way each of the moves, *a–h*, are represented in the kinetic Monte Carlo simulation shown in Table 1. The eight indices in the table specify the coordination number of the neighbors, labeled as indicated for some of the moves (b, d, e, f). The lower edge of the island, where edge diffusion process *e* takes place, is the B-edge. The upper edge, where kink attachment process *f* takes place, is the A-edge. (From Reference 65.)

types of stable step edges, and to be able to distinguish between attachment to a kink site and diffusion along a straight edge, just to name a couple of examples.

The next process to occur in a given configuration of the atoms in the system can be chosen by a uniformly distributed random number. A transition is picked according to the relative rate of processes in the table. One way to do this is to keep a running sum of the rates, $R_i = \sum_j^i r_j$. The random number, $0 \leq \nu \leq 1$, is then multiplied by the sum of all the rates, $R = \sum_i^M r_i$, and the process for which the running sum satisfies $R_{i-1} \leq \nu R \leq R_i$ becomes the next event to occur in the

TABLE 1 Examples of diffusion events on a FCC(111) surface and the description of each event in the kinetic Monte Carlo simulations presented in Figures 4–8[a]

Event		b	fb	fm	ff	cb	cm	cf	f
a	Hop on flat terrace	0	0	0	0	0	0	0	0
b	Attachment to A-edge	0	0	0	4	0	0	0	4
	Attachment to B-edge	0	0	0	0	0	0	4	4
c	Attachment to corner	0	0	0	0	0	0	0	4
d	Attachment to B-kink from terrace	0	0	0	3	0	0	3	4
e	Hop along B-edge	0	0	0	0	4	3	4	0
f	Attachment to A-kink from edge	0	4	3	4	0	0	0	3
g	Hop from A-edge to corner	0	4	3	0	0	0	0	0
h	Hop from corner site to B-edge	0	0	0	0	0	3	4	0
	Hop from corner site to B-kink	0	0	0	0	0	3	4	4

[a]Only hops between FCC sites are included in the event table, even though the transitions typically involve an intermediate, higher-energy hexagonal close packed (HCP) site. A set of eight indices specifies the environment of the initial and final sites of the moving atom. The index *c* refers to neighbors that are on the same side as the intermediate HCP site, the *f* designates the other side, and *b*, *m*, and *f* indicate whether the neighbor is in back, middle, or front site of each side (see Figure 2). The numerical value of each index specifies whether the particular neighbor is present and, if so, what its coordination number is. The convention used here is that neighbors of the moving atom are not included in the count. Parameters are given as integers, where 0 means the neighbor is absent, 1 means it is present but has no additional neighbors, 2 means it is present and has one additional neighbor, and so on. In practice, wild cards are used to specify any number larger than a given value. The numerical description is of the events shown in Figure 2.

system. The time elapsed until the next event occurs will on average be $\tau = 1/R$, but it may be important to include fluctuations in the time interval and estimate the time elapsed as

$$\tau = -\ln(\eta)/R,$$

where η is another random number between 0 and 1. After an event has occurred, the table of all possible events in the system will need to be updated because the configuration has changed. The table can be updated locally, modifying only the processes that are affected by the displaced atoms.

Essentially, the time increment in the kMC algorithm is the timescale of the fastest process in the system, $1/\mathrm{Max}\{r_i\}$. If this is on the order of a nanosecond, then a kMC simulation of surface growth can typically reach the timescale of a second in a week of computations. This becomes more and more difficult as the temperature of the system is raised. Sometimes, very fast processes that simply repeat themselves start to dominate and slow down the simulation. Several tricks have been proposed to eliminate such local equilibria. This problem becomes particularly severe in studies of island diffusion and evaporation. Metiu and coworkers have come up with a practical approach to deal with this by identifying separate timescales in the problem (66).

If little information is known about the processes in the system, it is possible to adjust the rates in the event table so as to make the kMC simulated results mimic

experimental data. This is, however, likely to lead to unphysical results because of the large flexibility in the simulation as compared with the constraints provided by a typical experimental data set. Many different kMC models have been known to fit the same experimental observations, but they disagree with each other and with more accurate estimates of the transition rates. It is important to start with first-principles estimates of the rates and limit the amount of fitting to just small adjustments in activation energy and/or prefactors. This first-principles approach has been used for Si adatom diffusion and island formation on Si(100) (47) and will likely be applied to other systems in the future as computational power increases and a full set of DFT estimates of the rates can be obtained more easily.

APPLICATION TO Pt(111) GROWTH

Perhaps the most intriguing observation in experimental crystal growth studies is the reentrant two-dimensional (2D) growth first reported by Kunkel et al (67–68a). Using reflectivity of a thermal He atom beam during vapor deposition of Pt, they observed a layer-by-layer, or 2D growth of the Pt surface at high temperature, 621 K. This is in the step-flow regime, where the surface remains nearly flat and highly reflective at all times. As the temperature was lowered to 424 K, the reflectivity dropped rapidly, indicating a rough surface and growth of three-dimensional (3D) structures. This is to be expected at low temperature, where the adatoms diffusing on the flat terrace do not make it to step edges, but rather congregate and form islands. The activation energy for processes that bring atoms down from atop islands can no longer be overcome and new islands form on top of existing islands instead of completing the layer. The unexpected observation was reappearance of near 2D growth as the temperature was lowered further, to 275 K. The first couple of layers appeared from the He reflectivity to spread on the surface nearly as well as in the high-temperature step-flow regime. This is counterintuitive and requires explanation in terms of atomic-scale dynamics. It is commonly desirable in technology to grow thin, smooth films on top of substrates at as low a temperature as possible to reduce interdiffusion, so this effect could possibly be useful. It is known from nucleation theory that nucleation of new islands starts at a lower density at lower temperature, thus creating more and smaller islands. Kunkel and coworkers speculated that the cause of the reentrant 2D growth could be found in "the reduced island size and/or their less regular shape, both due to the reduced adatom mobility at lower temperature" (67). As is discussed below, atomistic modeling has provided evidence that the less-regular shape of low-temperature islands is most important for the reentrant 2D effect.

Pushout Events

When a Pt atom in the vapor phase approaches a Pt surface, the attraction to the surface is strong enough to give the atom kinetic energy of several electron volts

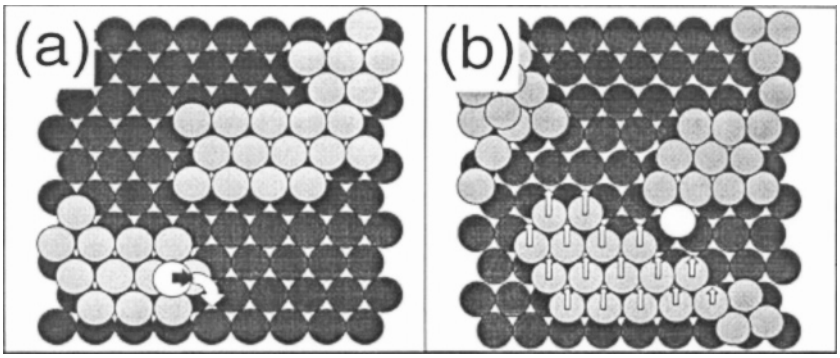

Figure 3 (*a*) A push-out event. A Pt vapor atom (*open circle*) lands on top of a Pt island (*light gray*) on the surface but ends up being incorporated into the island. An edge atom in the island gets pushed out, and the incoming atom takes its place. (*b*) A concerted annealing event. After deposition of an additional atom (*open circle*), an island that has largely been formed on hexagonal close packed sites shifts over to FCC sites. This kind of event would be hard to anticipate and include in the event table of a kinetic Monte Carlo simulation. (From Reference 69.)

by the time it is subject to the repulsive Pauli exclusion interaction with the surface atoms. Because the interaction between Pt atoms is soft and largely nondirectional, the collision can cause surface atoms to be pushed out of place. An example of this is shown in Figure 3*a*. Here the incoming atom is incident on a site adjacent to the edge of an island. The incoming atom imparts momentum on the surface atom, which gets displaced and the incoming atom takes its place. This kind of "push-out" event was observed in direct classical dynamics simulations of deposition using an EAM potential (69). Similar results were obtained for Cu deposition on Cu(111) using an EMT interaction potential (70). For vapor deposition, only the sites adjacent to the edge lend themselves to push out, so this effect is more important the smaller the islands are. It could therefore contribute to reentrant 2D growth. However, the probability of push out is not large enough to cause the reentrant 2D growth in Pt(111); the Pt islands are too large even at 275 K (50, 71).

In sputter deposition, which is a common way of growing thin films, the deposited atoms are incident with energy on the order of 10–20 eV. At this high energy, the cross section for push out is much larger. A push-out event can occur even when the incident atom lands near the third site in from the edge (71). The mechanism sometimes involves concerted motion of several atoms, as was revealed in MEP calculations that used the final states obtained from the deposition simulations. At 20 eV, exchange processes with the terrace atoms start becoming active.

Despite the large acceleration of the incident atoms toward the surface, the thermal equilibration is fast, and the newly deposited atom loses its excess energy within a couple of vibrational periods (50). The deposited atom therefore tends to land very near the site of impact, i.e. there is little or no transient mobility at

the surface (72, 72a). The momentum transfer between the incoming atom and a surface atom is highly effective because their mass is equal and the vibrational coupling between adjacent atoms in the lattice is relatively weak.

Figure 3*b* shows a concerted annealing event that was observed in classical dynamics simulations of Pt deposition (69). After the deposition of a Pt atom near an island that initially formed with a grain boundary [with approximately half the island atoms at hexagonal close-packed (HCP) sites], the island moves in an amoeba-like fashion and anneals to a purely FCC island. Although this particular event is possible only in a classical dynamics simulation because the EAM potential function used has low diffusion barrier and too strong binding energy at HCP sites, it illustrates the difficulty in creating kMC tables that include all relevant events. It would be hard to guess this kind of process would take place, and it would be practically impossible to include it in a manageable kMC classification scheme of events. This emphasizes the importance of long time simulation methods that do not require prior knowledge of the relevant processes.

Island Shape

The shape of islands on a growing surface can give information about the dynamics of the surface atoms. STM measurements of Michely and coworkers have given a wealth of information about the shape of islands on the Pt(111) surface (73–75).

At low temperature, the islands are irregular and dendritic. This is reminiscent of so-called diffusion-limited aggregates (76, 76a), but here the arms are thicker because some annealing processes are active. As the temperature is raised, the arms gradually become thicker (75). kMC simulation results shown in Figure 4 illustrate these types of islands (65). The figure illustrates the effect of making the attachment barrier to a kink site smaller than the diffusion barrier at a straight step edge, a feature predicted by EAM calculations. Because of the irregular shape, a great number of different local environments are found and quantitative analysis of the branch thickness is likely to require an extensive table of transitions in the kMC simulations.

A particularly intriguing feature is the observation of a triangular envelope around the dendritic islands. A similar and stronger effect has been observed in Ag overlayer growth (77, 78). One mechanism that can explain this is asymmetry in the barrier to escape from a corner site to an edge site (similar to site *h* in Figure 2*b*) (75). An envelope with sides aligned with B-edges (see Figure 2*b* for illustration of A- and B-edges) develops if it is easier to hop from a corner site to an A-edge than a B-edge. kMC simulations were fitted to the Pt(111) experimental data by including this effect (75). However, recent DFT calculations (18) have given an asymmetry in the corner escape barriers that is in the wrong direction and of much smaller magnitude than was deduced from the kMC fit (75). Another possible way of obtaining such a triangular envelope was suggested by Brune (2). If attachment to one of the two edges has a barrier, or upward drift in site energy, then adatoms will preferably attach to the other edge. Figure 5 shows the results

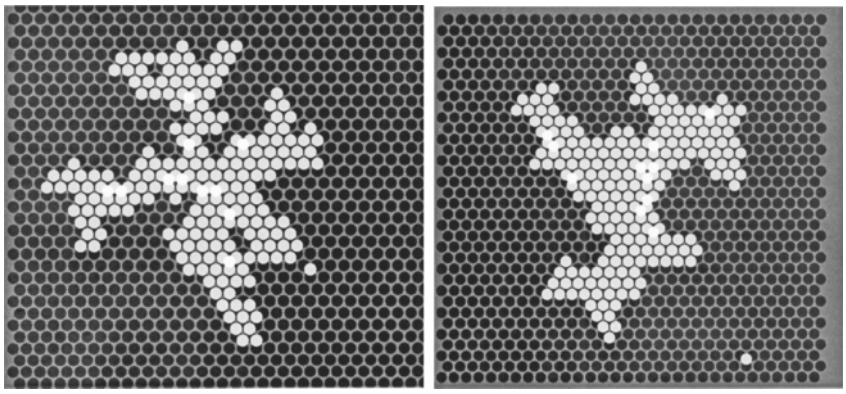

Figure 4 Dendritic islands obtained from kinetic Monte Carlo simulations with a deposition rate of 10^{-3} monolayers/s. While adatom diffusion along straight edges, $E_a = 0.7$ eV, is not active at this low temperature, $T = 200$ K, the hop from a corner site to an edge is active, $E_a = 0.2$ eV, and leads to thickening of the arms. (*Left*) The barrier for all for edge diffusion hops is $E_a = 0.7$ eV. (*Right*) The barrier for attachment to a kink site is lowered to 0.45 eV. This leads to significant thickening of the arms. (From Reference 65.)

of a kMC simulation where the attachment to a B-edge has a higher barrier than attachment to an A-edge. A clear triangular B-edge envelope is produced (79). It is unclear at this time what the triangular envelope observed in Pt islands is due to.

At higher temperature, when the diffusion along step edges and crossing from one edge to another becomes active, the islands become compact. Michely and coworkers observed triangular compact islands at 400 K with A-edges (73, 73a). This has recently been shown to be an artifact of very slight CO contamination (74). In the absence of CO (when the partial pressure of CO is brought to or below 10^{-11} mbar), the islands are triangular with B-edges. A partial pressure of only 10^{-19} mbar is enough to reverse the triangular envelope of the islands completely. The reason is that CO preferably adsorbs on the undercoordinated atoms at the step edges. The triangular islands can easily be reproduced in kMC simulations by making the binding energy of Pt adatoms slightly greater on one edge than the other (65, 80). Figure 6 shows an island grown where the binding at a B-edge is only 0.04 eV (65). The energy landscape used in these simulations was obtained from EAM calculations initially, but then adjusted to match experimentally measured diffusivity (55) and the observed island shapes in the temperature range of 205–455 K (the older, CO-contaminated data). The landscape is shown in Figure 7*a*. This slight energy preference for the B-edge is enough to increase the population of adatoms at the edge significantly (by nearly a factor of 10 according to Boltzmann statistics), thereby increasing the growth rate of the B-edge and leaving the island with A-edges. This illustrates that overall morphology of surface features can be dominated by very small energy differences (smaller than the typical error bars in DFT calculations).

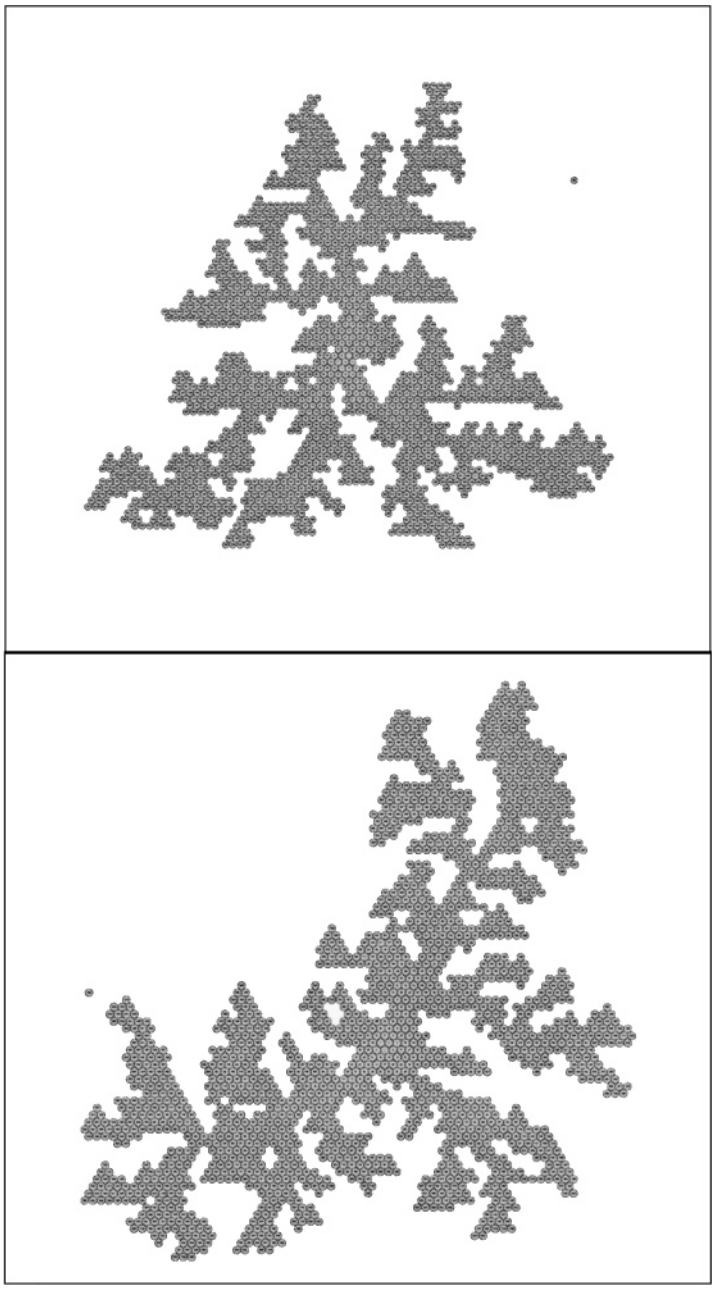

Figure 5 Dendritic islands grown with a deposition rate of 10^{-3} monolayers/s at 250 K. The edge diffusion barriers are the same as in Figure 4, but here the attachment of an adatom to the edge has a barrier of 0.20 eV at the A-edge and 0.30 at the B-edge, whereas the diffusion barrier on the flat terrace is 0.25 eV. A triangular envelope develops around the island, with sides parallel to the B-edge. Two islands are shown, differing only in the random numbers used in the kinetic Monte Carlo simulation. (From Reference 79.)

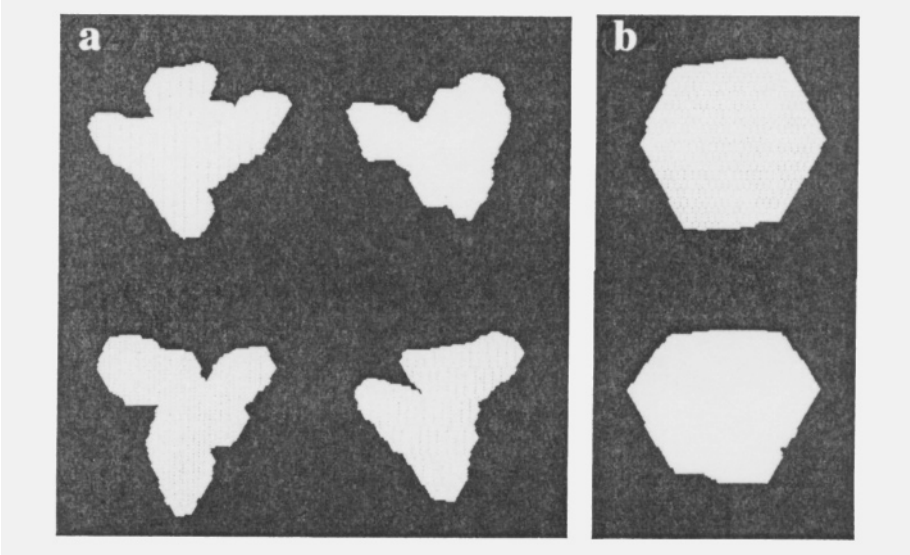

Figure 6 Islands grown with the same deposition rate as in Figure 4. (*a*) $T = 400$ K; an area of 770 Å $\times$ 1100 Å is shown. (*b*) $T = 455$ K; an area of 350 Å $\times$ 700 Å is shown (each island has ca 5000 atoms). The potential energy landscape is shown in Figure 7*a*. (From Reference 65.)

The reentrant 2D growth effect mentioned above does not rely on the formation of CO-contaminated islands with A-edges at the intermediate temperature. In fact, the more recent STM images show that, the cleaner the system is, the stronger the reentrant 2D effect (81). The He scattering experiments that originally identified the reentrant 2D growth mode (67, 68) were carried out at a 10^{-11} mbar pressure so the surface was likely not CO contaminated.

Another effect that controls the relative growth rate of the two edges is the diffusivity along an edge (65, 80). The important question is, on which edge is a dimer of adatoms more likely to form? The adatom explores more of the edge with the lower edge diffusion barrier. This increases the probability of finding a kink or forming a dimer with another adatom on the edge with faster diffusion. The adatom tends to be reflected back to the edge at a corner site if it is on the edge with the lower diffusion barrier. In the energy landscape shown in Figure 7*a*, the diffusion barrier at the A-edge is lower, favoring growth of the A-edge. This opposes the binding energy preference for the B-edge, and at 455 K the two balance each other out and the resulting island shape is nearly hexagonal (see Figure 6*b*), in agreement with the STM measurements on CO-contaminated islands (73, 73a).

At higher temperature, a difference in the dissociation energy of dimers at the two edges can affect the relative growth rate of the edges (80). Likely, there are several other factors that can play a role in determining island shapes.

Michely et al (73, 73a) again observed triangular islands at still higher temperature, at 640 K, but now oriented in the opposite way compared with the triangular

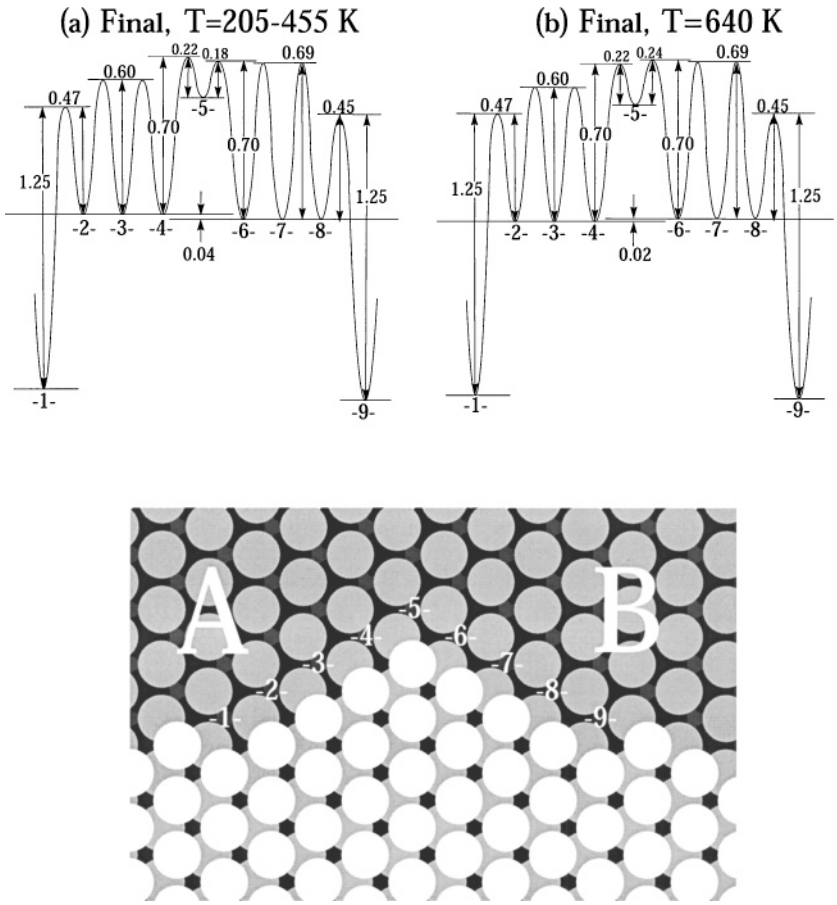

Figure 7 Potential energy landscape deduced by comparing kinetic Monte Carlo simulations with scanning tunneling microscopy (STM) measurements. The potential well farthest to the *left*, labeled *1*, represents binding to a kink on the A-edge. The three potential wells to the *right*, labeled *2–4*, represent binding at the A-edge. The central well, labeled *5*, represents binding to a corner site. The potential wells labeled *6–8* represent binding to the B-edge. The well labeled *9* represents binding to a kink on a B-edge. (*a*) Barriers fitted to reproduce STM images taken at $T = 205$ K to $T = 455$ K. There is a slight binding energy preference of 0.04 eV for the B-edge. This landscape was used in the simulations shown in Figure 6. (*b*) A slight modification to the energy landscape in panel *a* was needed in order to reproduce the islands observed at 640 K. Now there is a slight binding energy preference, 0.02 eV, for an adatom at the A-edge. This landscape was used in the simulations shown in Figure 8. More recent experiments have shown that the low-temperature measurements were made on a CO-contaminated system, but the CO desorbs at around 500 K, explaining the change in the deduced energy landscape. (From Reference 65.)

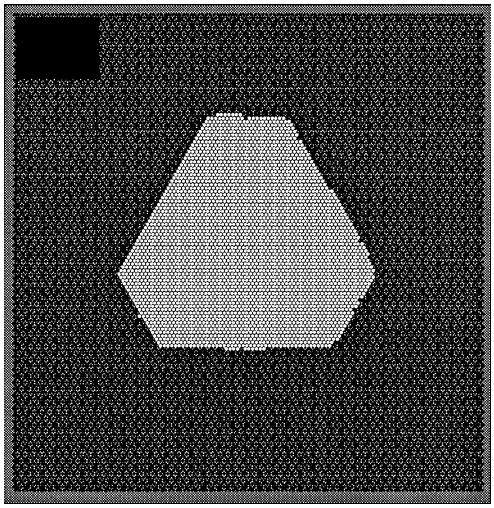

Figure 8 An example of an island grown at $T = 640$ K with the same deposition rate as in Figure 4. The island contains 9000 atoms. The potential energy landscape is shown in Figure 7*b*. (From Reference 65.)

islands at 400 K, the high-temperature islands have B-type edges. Villarba (65) had tried to reproduce this feature in an energy landscape consistent with the lower temperature range but concluded that there had to be a slight change in the energy landscape in the temperature interval of 455–640 K. Figure 7*b* shows the higher-temperature landscape and Figure 8 shows the simulated island shape, which is in good agreement with the STM measurements (73, 73a). Most important, the binding energy preference is now changed to favor the A-edge by 0.02 eV, a shift of only 0.06 eV from the lower-energy landscape, again illustrating how very slight energy changes can dramatically alter the island shape. Since the discovery of the CO contamination, it is now evident that this change in the landscape is due to the desorption of the CO molecules from the surface, which is known to occur at about 500 K (81).

It is important to emphasize that all these island shapes are determined by nonequilibrium processes. The equilibrium island shape is not reached for these deposition rates until 750 K, where nearly hexagonal islands with slightly longer B-edges are formed.

Little attention has so far been paid to the possible size and flux dependence of island shapes. A recent kMC study has identified a mechanism by which the island shape can transform from one triangular shape (for example with mainly A-edges) to the other (with mainly B-edges) as the size of the island increases (79). This does not appear to happen in Pt(111) island growth, but it may be relevant in other systems.

The Ehrlich-Schwoebel Barrier

An important feature of the energy landscape that determines whether the growth of islands is 2D or 3D is the energy barrier for descent of adatoms from atop islands. Simple bond counting arguments can be used to demonstrate that such a barrier

is likely to exist. If an adatom were to hop over the island edge, it would need to give up one of the three bonds it forms with underlying atoms, thereby creating a high-energy transition state. EAM (50), EMT (83), and DFT (34) calculations predict that the descent process involves concerted exchange rather than hop, but an energy barrier is still predicted to be present. An atom that lands on top of an island, therefore, faces a wall along the edge of the island, and at low enough temperature, adatoms accumulate on top of the island and nucleate a new island, thereby leading to 3D growth. The existence of such a barrier was predicted by Schwoebel & Shipsey (84) and inferred from experiments by Ehrlich & Hudda (84a) and is now usually referred to as the Ehrlich-Schwoebel (ES) barrier. The important question is what the additional barrier to descent is in comparison with reflection of the adatom back to the interior of the island. The precise definition of the ES barrier is discussed in more detail below.

Because of the observation of the surprising reentrant 2D growth in Pt(111) (67–68a), there has been a great deal of work devoted to the study of adatom descent, or interlayer transport. Many subtle features of the energy landscape can affect the probability of descent. An EAM calculation of the energy landscape for an adatom approaching a step edge from above showed significant deviations from the flat terrace energy landscape several sites away from the edge (50). A gradual rise in the energy (decrease in the binding energy) was observed for sites as far as three sites away from the edge. This is due to elastic strain caused by the step. This is a subtle effect, but even a rise of only 0.03 eV will significantly reduce the population of adatoms at the sites near the edge. Gölzhäser & Ehrlich have, indeed, observed such an excluded zone near the edges of a Pt island on Pt(111) in FIM experiments (85).

At the site adjacent to and above the step edge the EAM calculations showed stronger bonding than at the flat terrace (50). This can be understood from bond-counting arguments (86). Less-coordinated atoms form stronger bonds. The edge atoms are only sevenfold coordinated as compared with ninefold coordination of terrace atoms. The adatom, therefore, binds more strongly at the edge sites. This effect has been observed in FIM experiments by Wang & Ehrlich (87). This effect leads to interesting dynamics where the adatom preferably diffuses along the edge once it has reached the edge. This increases the attempt frequency for descent but also increases the probability of nucleation on top of the island. Results of classical dynamics simulations using the EAM potential are shown in Figure 9 (50). At the lower temperature, this causes the adatom to be bound to the edge, but it can still diffuse along the edge. Also, the barrier for hopping one site away from the edge is considerably smaller than the barrier for hopping from one terrace site to another. The adatom can therefore have excursions to the second site without really leaving the edge. This illustrates that one has to be careful when defining the ES barrier. It should reflect the relative probability of descent vs reflection back into the interior of the island. The relevant quantity is the height of the transition state for descent minus the height of the highest transition state for diffusion away from the edge on the upper terrace with respect to a common zero of energy, which can be taken as the binding energy at the edge site. It may not be sufficient to define the ES barrier

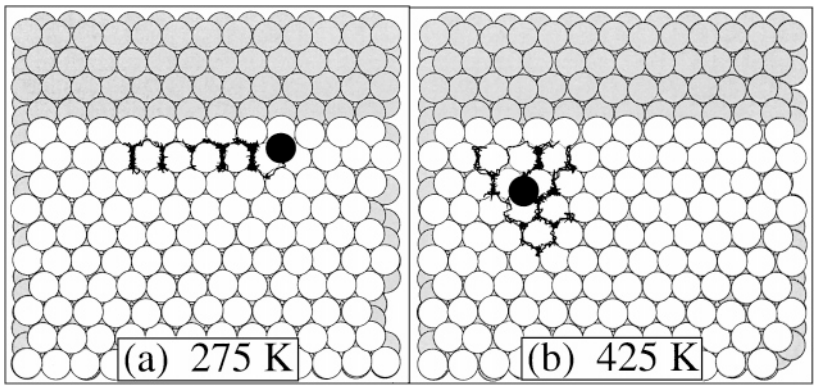

Figure 9 Dynamics of an adatom on top of an island near the island edge, calculated using an EAM potential function. (*a*) At low temperature, the adatom is trapped in a potential energy trough that forms near the edge because of stronger bonding to the undercoordinated edge atoms. The adatom diffuses primarily along the edge. (*b*) At higher temperature, the adatom can escape more easily from the edge region. Density functional theory calculations show an even stronger attraction to the edge sites. (From Reference 50.)

simply as the difference in barrier for descent minus the barrier to hop from the edge site to the site second from the edge.

DFT/LDA calculations by Feibelman have shown an even stronger attraction to the descending edge (34). The adatom was found to bind 0.24–0.26 eV more strongly at the edge site than to the second site from the edge. Because the size of the system studied by DFT is very small, it is not possible to tell what the binding energy at the edge is with respect to terrace sites. The diffusion barrier for hopping along the edge is calculated in DFT to be significantly lower (by over 0.1 eV) than either the barrier for descent or the barrier for a hop to the second site from the edge. An adatom that has reached the edge is therefore most likely going to run along the perimeter of the island for a long time, sampling both A- and B-edges. A key question is what the relative energy of the A- and B-edge sites is. This is hard to establish from DFT calculations because of the small system size. It can be argued that the B-edge is likely to bind stronger than the A-edge. The adatom binds to two undercoordinated edge atoms at the B-edge FCC sites, but only one at the A-edge. Because an adatom running along the edge will likely equilibrate between the A- and B-edges, a 0.1-eV binding preference for the B-edge (which can be justified on the basis of bond counting arguments, see below) would have a large effect on the relative population of the edge sites. Also, if the B-edge site is lower in energy by such an amount, then the saddle point energy for descent at the two edges calculated by DFT/CDA (34) is similar when compared with a common energy reference. More work is being done currently to resolve this issue.

As the adatom runs along the edge, it is likely to encounter defects on the edge, in particular kinks. The importance of kinks in the descent process was first

pointed out by Villarba & Jónsson based on studies in which the EAM potential was used (50, 69). It was shown that kink sites can offer significantly lower energy pathways for descent compared with straight edges [A study based on "corrected EMT" potential function reached the opposite conclusion: that kink sites did not offer lower-energy pathways for adatom descent (88). A later paper by the same authors reversed that conclusion (88a)]. An unexpected mechanism that involves an edge atom near, but not at, a kink site on the B-edge turned out to have a particularly low-energy barrier. Recent DFT/PW91 calculations have shown that this qualitative feature predicted by the EAM calculations is retained in the first-principles calculations (89). Figure 10 shows the calculated energy along the MEP for this process, as well as an exchange with the kink atom. The sequence of replicas along the path obtained by the NEB is shown for both processes (*inset*, Figure 10*b,c*). The remarkable thing is that the process with the lower activation energy is the process leading to a significantly higher-energy final state, an atom with only fivefold coordination, as compared with the sixfold coordination of an atom at the kink site. This illustrates that the simple and commonly used rule of scaling barriers with the energy of the final state can be a drastic oversimplification and can lead to incorrect prediction of the surface dynamics and morphology. The DFT results in Figure 10 also illustrate the variation in the binding energy as the adatom moves along the edge. Both curves start from the high-energy site where the adatom binds to the eightfold coordinated kink atom and two ninefold coordinated terrace atoms (no edge atoms). Before the process illustrated in Figure 10*a*, the adatom hops to an edge site where the coordination of the three underlying neighbors is 7, 8, and 9. Before the process in Figure 10*b*, the adatom hops to a site where the coordination of underlying neighbors is 6, 7, and 9. This turns out to be the most stable site along the edge, more stable by 0.06 eV than a site at the straight edge. The initial state for the unexpected descent process shown in Figure 10*a* i*s*, therefore, particularly likely, and this will increase the probability of these kinds of events. These calculations also indicate that an increase or decrease in the coordination of the underlying neighbors translates to about a 0.07-eV change in the binding energy, which suggests that the A-edge sites are ca 0.14 eV higher in energy than the B-edge sites.

An atomic scale mechanism for the reentrant 2D growth was given by Villarba & Jónsson (50) based on their EAM barrier calculations. They reached the conclusion that the transition from 3D growth to 2D growth as the temperature is lowered is due to the change in island shape (50). The transition coincides with a transition from compact triangular islands (with large ES barriers) at higher temperature to dendritic islands with a large density of kink sites (and therefore "holes" in the ES barrier) at the lower temperature. Thus, even though the thermal energy of the adatoms is reduced, the number of holes in the ES barrier is increased enough by the increase in kink density that 2D growth reappears as the temperature is lowered. This is consistent with the original explanation of Kunkel et al (67), but more specific.

Simulations of Pt(111) growth using the kMC approach were carried out by Jacobsen et al (83). They were able to reproduce reentrant 2D growth in their

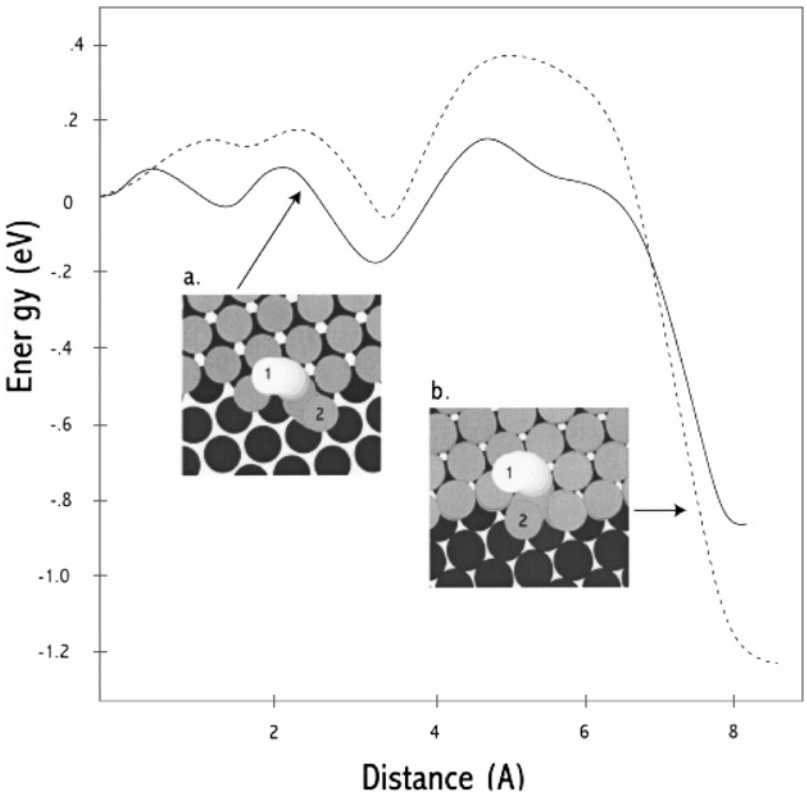

Figure 10 Density functional theory PW91 calculations of the minimum energy path for descent of an adatom near a kink site on the B-edge. Two paths are shown. (*a*) Final state with significantly higher energy but lower activation barrier than (*b*). In both cases, the adatom starts in a high-energy site, bonded to the eightfold coordinated atom at the kink as well as two ninefold coordinated atoms. (*Solid line*) Corresponds to a hop (via a hexagonal close packed site) to the site marked *1* in Figure 10*a*, where the adatom binds to a sixfold coordinated atom and then undergoes an exchange descent as shown by the nudged elastic band (NEB) path in Figure 10*a*. At the end of this process an edge atom has been pushed to a fivefold coordinated site. (*Dashed line*) Corresponds to a hop to the site marked *1* in Figure 10*b*, where the adatom binds to a sevenfold coordinated atom and then undergoes an exchange descent as shown by the NEB path in Figure 10*b*. At the end of this process, an eightfold kink atom has been pushed to a sixfold coordinated site. The attempt frequency for (*a*) is high because the initial state for the exchange is the most stable site along the B-edge. Qualitatively similar results were obtained with the empirical EAM potential (See Reference 50.)

simulations. They concluded that no reasonable set of barriers and prefactors could reproduce the reentrant 2D growth unless the kink descent process shown in Figure 10*a* was included. The simulations were tailored to the CO-contaminated STM experiments where triangular islands with A-edges form in the intermediate 3D growth regime. The more recent CO-free STM experiments, which show even stronger reentrant 2D behavior in the absence of A-edged triangular islands, have not yet been reproduced in kMC simulations.

Several studies of Pt diffusion rates have been carried out in addition to those mentioned above, in particular to study island diffusion (90–90d).

FUTURE DIRECTIONS

The example discussed above illustrates that a number of important processes, some subtle and unexpected, control the surface morphology of a growing crystal. The challenge to theoretical studies in this area is to identify the relevant processes and estimate the rate of these processes accurately enough to be able to explain the surface patterns observed in experimental measurements.

This is, indeed, a challenging problem both for experiment and theory. Even minute amounts of impurity in laboratory studies have been shown to change the patterns formed on a growing surface drastically. In the dynamics simulations, even a slight change in relative energy, well within typical error bars of the first-principles calculations, can tilt the balance between competing processes and dramatically change the simulated results.

The most serious challenge to the theoretical studies is the problem of identifying the relevant processes. As the Pt(111) example illustrates, the key process may be nonintuitive (as the process shown in Figure 10*a*). The most pressing problem is to develop algorithms that can find what processes would occur in the simulated system if the direct classical dynamics simulations could be carried out long enough to cover experimental timescales. The recently proposed accelerated dynamics techniques are promising, but they need to be applied to large problems and may need to be developed further, or better methods may need to be discovered.

The kMC simulations work well at low-enough temperature and for small-enough systems. The problem with fast, repeating processes that slow down the time evolution in the simulation has been addressed in several ways, but a more systematic method for dealing with this problem may be possible and would certainly be useful. It should be possible to develop algorithms where previously visited configurations are recognized and repeated cycling between configurations identified and dealt with as a local equilibrium. A generally applicable algorithm would be desirable, rather than fixes for particular cases.

Molecular level simulations can be extended to larger length scales by using parallel computers. A straightforward way of doing this is to divide the system into spatial cells and use one processor per cell. However, there is a limit to the length scale that can be simulated in this way, and more important, this is inefficient in the sense that many more degrees of freedom are being used to describe the

system than is necessary. A more efficient approach to reach mesoscopic scales would be to invoke a continuum description of the system. For example, in order to simulate the roughness of the surface and the shape of islands and other structures formed on the surface during crystal growth, it would be more efficient to invoke a continuous function that gives the height of the surface as a function of the lateral position. The effect of diffusion and other dynamics could then be represented by a set of differential equations. The challenge is to (*a*) determine the form of the equations and parameters that are consistent with the molecular scale dynamics, (*b*) rigorously extrapolate microscopic physical phenomena to macroscopic scales, and (*c*) incorporate singularities that arise from strictly atomistic phenomena (such as facets and corners) into the mathematics of continuum behavior.

The challenge of explaining how microscopic processes influence macroscopic behavior is particularly relevant in studies of growth shapes of crystals, which offer a unique testing ground for the computational challenges of bridging vast length scales and timescales. The advantage of continuum models, such as phase field models (91–94), is their computational simplicity. The challenge is to provide a rigorous link between microscopic (atomistic) modeling and continuum modeling. Microscopic simulations (classical trajectories and kMC) can be used to test and refine continuum models. The results of the microscopic simulations can be used in this context as "experimental" data, where it is known exactly what microscopic events occur. Ultimately, the results of the continuum models could be compared with experimental results, thereby testing whether the right microscopic dynamics have been accounted for in the construction of the continuum models.

ACKNOWLEDGMENTS

I would like to thank the many researchers in my group who have worked on the methodology and carried out the simulations that are the focus of this review. Particular thanks go to Daniel Faken, Graeme Henkelman, Greg Mills, Grace Siswanto, and Marie Villarba. Numerous discussions and, in some cases, collaborations with Peter Feibelman, Karsten Jacobsen, Ken Jordan, Horia Metiu, Thomas Michely, Jens Nørskov, Bene Poelsema, and Art Voter are gratefully acknowledged. Support came from National Science Foundation grant numbers CHE-9710995 and CHE-9217774.

LITERATURE CITED

1. Levinthal C. 1969. In *Mossbauer Spectroscopy in Biological Systems*, ed. P Debrunner, J Tsibris, E. Munck, pp. 22–24. Urbana, IL: Univ. Ill. Press
2. Brune H. 1998. *Surf. Sci. Rep.* 31:121
3. Poelsema B, Comsa G. 1989. *Scattering of Thermal Energy Atoms from Disordered Surfaces. Springer Tracts in Modern Physics,* Vol. 115. Berlin: Springer-Verlag
4. Van Hove JM, Lent CS, Pukite PR,

Cohen PI. 1983. *J. Vac. Sci. Technol.* B1: 741
4a. Larsen PK, Dobson PJ. 1987. In *Reflection High-Energy Electron Diffraction and Reflection Electron Imaging of Surfaces. NATO ASI Ser.* Ser. B, Vol. 188. New York: Plenum
5. Kohn W, Becke AD, Parr RG. 1996. *J. Phys. Chem.* 100:12974
6. Berne BJ, Ciccotti G, Coker DF. 1998. See Ref. 95
7. Bassett DW, Webber PR. 1978. *Surf. Sci.* 70:520
8. Mo Y-W, Kleiner J, Webb MB, Lagally MG. 1991. *Surf. Sci.* 268:275
9. Campbell CT. 1997. *Surf. Sci. Rep.* 227:1
10. Smith RS, Kay BD. 1997. *Surf. Rev. Lett.* 4:781
10a. Morgenstern M, Müller J, Michely T, Comsa G. 1997. *Z. Phys. Chem.* 198: 43
11. Kamins TI, Medeiros-Ribeiro G, Ohlberg DDA, Williams RS. 1999. *J. Appl. Phys.* 85:1159
12. Li Y, Wahnström G. 1992. *Phys. Rev. Lett.* 68:3444
12a. Li Y, Wahnström G. 1992. *Phys. Rev. B* 46:14528
13. Hohenberg P, Kohn W. 1964. *Phys. Rev.* 136:B864
13a. Kohn W, Sham LJ. 1965. *Phys. Rev.* 140:A1133
14. Brocks G, Kelly PJ, Car R. 1991. *Phys. Rev. Lett.* 66:1729
14a. Smith AP, Jónsson H. 1996. *Phys. Rev. Lett.* 77:1326
15. Stumpf R, Scheffler M. 1994. *Phys. Rev. Lett.* 307:501
15a. Stumpf R, Scheffler M. 1996. *Phys. Rev. B* 53:4958
15b. Lee C, Barkema GT, Breeman M, Pasquarello A, Car R. 1994. *Surf. Sci.* 306:L575
16. Kresse G, Furthmüller J. 1996. *Comp. Mat. Sci.* 6:16
16a. Kresse G, Furthmüller J. 1996. *Phys. Rev. B* 55:11169
17. Hammer B, Hansen LB, Nørskov JK. 1999. *Phys. Rev. B* 59:7413
18. Feibelman PJ. 1999. *Phys. Rev. B* 60:4972
19. Bachelet GB, Hamann DR, Schluter M. 1982. *Phys. Rev. B* 26:4199
20. Vanderbilt D. 1990. *Phys. Rev. B* 41:7892
21. Hernandez E, Gillan MJ, Goringe CM. 1996. *Phys. Rev. B* 53:7147
21a. Hierse W, Stechel EB. 1994. *Phys. Rev. B* 50:17811
21b. Ordejon P, Artacho E, Soler JM. 1996. *Phys. Rev. B* 53:R10441
22. Becke AD. 1988. *Phys. Rev. A* 38:3098
23. Lee C, Yang W, Parr RG. 1988. *Phys. Rev. B* 37:785
24. Perdew JP, Chevary JA, Vosko SH, Jackson KA, Pederson MR, et al. 1992. *Phys. Rev. B* 46:6671
25. Smith A, Wiggs J, Jónsson H, Yan H, Corrales LR, et al. 1995. *J. Chem. Phys.* 102:1044
26. Pople JA, Head-Gordon M, Raghavachari K. 1987. *J. Chem. Phys.* 87:5968
27. Swartzentruber BS, Smith AP, Jónsson H. 1996. *Phys. Rev. Lett.* 77:2518
28. Nachtigall P, Jordan KD, Smith A, Jónsson H. 1996. *J. Chem. Phys.* 104:148
29. Hansen L, Stoltze P, Jacobsen KW, Nørskov JK. 1991. *Phys. Rev. B* 44:6523
29a. Jacobsen KW. 1988. *Comments Condens. Mat. Phys.* 14:129
30. Daw MS, Baskes MI. 1984. *Phys. Rev. B* 29:6443
30a. Daw MS. 1989. *Phys. Rev. B* 39:7441
31. Voter AF, Chen SP. 1987. *Mat. Res. Soc. Symp. Proc.* 82:175
32. Stillinger FH, Weber TA. 1985. *Phys. Rev. B* 31:5262
32a. Tersoff J. 1988. *Phys. Rev. B* 37:6991
32b. Bolding BC, Andersen HC. 1990. *Phys. Rev. B* 41:10568
33. Liu CL, Cohen JM, Adams JB, Voter AF. 1991. *Surf. Sci.* 253:334
34. Feibelman PJ. 1998. *Phys. Rev. Lett.* 81:168
35. Batista E, Jónsson H, Xantheas S. 1998. *J. Chem. Phys.* 109:4546

35a. Batista E, Xantheas S, Jónsson H. 1999. *J. Chem. Phys.* 111:6011
35b. Batista E, Xantheas S, Jónsson H. 2000. *J. Chem. Phys.* 112:3285
36. Pechukas P. 1976. In *Dynamics of Molecular Collisions*, Part B, ed. WH Miller, pp. 269–322. New York: Plenum
36a. Truhlar DG, Garrett BC, Klippenstein SJ. 1996. *J. Phys. Chem.* 100:12771
37. Keck JC. 1967. *Adv. Chem.* 13:85
38. Voter AF, Doll D. 1984. *J. Chem. Phys.* 80:5832
39. Truhlar DG, Garrett BC. 1984. *Annu. Rev. Phys. Chem.* 35:159
40. Voter AF, Doll D. 1985. *J. Chem. Phys.* 82:80
41. Jóhannesson G, Jónsson H. Submitted for publication
42. Mills G, Jónsson H, Schenter GK. 1995. *Surf. Sci.* 324:305
43. Feibelman PJ. 1990. *Phys. Rev. Lett.* 65:729
44. Kellogg GL, Feibelman PJ. 1990. *Phys. Rev. Lett.* 64:3143
45. Wert C, Zener C. 1949. *Phys. Rev.* 76:1169
45a. Vineyard GH. 1957. *J. Phys. Chem. Solids* 3:121
46. Kellogg GL. 1994. *Surf. Sci. Rep.* 21:1
47. Smith AP, Jónsson H. 1996. *Phys. Rev. Lett.* 77:1326
48. Jónsson H, Mills G, Jacobsen KW. 1998. See Ref. 95, p. 385
49. Henkelman G, Jónsson H. Submitted for publication
50. Villarba M, Jónsson H. 1994. *Surf. Sci.* 317:15
51. Uberagua B, Levskovar M, Smith AP, Olmstead M, Jónsson H. 2000. *Phys. Rev. Lett.* 84:2441
52. Cerjan CJ, Miller WH. 1981. *J. Chem. Phys.* 75:2800
53. Simons J, Jørgensen P, Taylor H, Ozment J. 1983. *J. Phys. Chem.* 87: 2745
53a. Nichols J, Taylor H, Schmidt P, Simons J. 1990. *J. Chem. Phys.* 92:940
54. Wales DJ. 1989. *J. Chem. Phys.* 91:7002
55. Henkelman G, Jónsson H. 1999. *J. Chem. Phys.* 111:7010
56. Voter AF. 1997. *J. Chem. Phys.* 106:4665
56a. Voter AF. 1997. *Phys. Rev. Lett.* 78:3908
56b. Voter AF. 1998. *J. Chem. Phys.* 57: R13985
57. Voter AF, Germann TC. 1998. *Mat. Res. Soc. Symp. Proc.* 528:221
58. Sørensen MR, Jacobsen KW, Jónsson H. 1996. *Phys. Rev. Lett.* 77:5067
59. Voter AF, Sørensen M. 1999. *Mat. Res. Soc. Symp. Proc.* 538:427
59a. Sørensen M, Voter AF. 2000. *J. Chem. Phys.* In press
60. Gillespie DT. 1976. *J. Comp. Phys.* 22: 403
60a. Gillespie DT. 1977. *J. Phys.* 81:2340
60b. Gillespie DT. 1978. *J. Comp. Phys.* 28:395
61. Gilmer GH. 1980. *Science* 208:355
62. Voter AF. 1986. *Phys. Rev. B* 34:6819
63. Fichthorn KA, Weinberg WH. 1991. *J. Chem. Phys.* 95:1090
64. Voter AF. 1987. *SPIE Model. Opt. Thin Films* 821:214
64a. Breeman M, Barkema GT, Langelaar MH, Boerma DO. 1996. *Thin Solid Films* 272:195
65. Villarba M. 1995. *Atomic scale processes relevant to metal crystal growth*. PhD thesis. Univ. Washington, Seattle. 140 pp. (Available from UMI, Ann Arbor, MI.)
66. Mills G, Mattsson TR, Mollnitz I, Metiu H. 1999. *J. Chem. Phys.* 111:8639
67. Kunkel R, Poelsema B, Verheij LK, Comsa G. 1990. *Phys. Rev. Lett.* 65:733
68. Poelsema B, Kunkel R, Nagel N, Becker AF, Rosenfeld G, et al. 1991. *Appl. Phys.* A 53:369
68a. Poelsema B, Becker A, Rosenfeld G, Kunkel R, Nagel N, et al. 1992. *Surf. Sci.* 272:269
69. Villarba M, Jónsson H. 1994. *Phys. Rev. B* 49:2208
70. Stoltze P, Nørskov J. 1993. *Phys. Rev. B* 48:5607

71. Villarba M, Jónsson H. 1995. *Surf. Sci.* 324:35
72. Sanders DE, DePristo AE. 1991. *Surf. Sci.* 254:341
72a. Sanders DE, Halstead DM, DePristo AE. 1992. *J. Vac. Sci. Technol.* A10:1986
73. Bott M, Michely T, Comsa G. 1992. *Surf. Sci.* 272:161
73a. Michely T, Hohage M, Bott M, Comsa G. 1993. *Phys. Rev. Lett.* 70:3943
74. Kalf M, Comsa G, Michely T. 1998. *Phys. Rev. Lett.* 81:1255
75. Hohage M, Bott M, Morgenstern M, Zhang Z, Michely T, Comsa G. 1996. *Phys. Rev. Lett.* 76:2366
76. Witten TA, Sander LM. 1981. *Phys. Rev. Lett.* 47:1400
76a. Meakin P. 1983. *Phys. Rev. A* 27:1495
77. Brune H, Röder H, Bromann K, Kern K, Jacobsen J et al.1996. *Surf. Sci.* 349:L115
78. Brune H, Romainczyk C, Roder H, Kern K. 1994. *Nature* 369:469
79. Siswanto G, Faken D, Jónsson H. Submitted for publication.
80. Jacobsen J, Jacobsen KW, Nørskov J. 1996. *Surf. Sci.* 359:37
81. Michely T. Personal communication
82. Deleted in proof
83. Jacobsen J, Jacobsen KW, Stoltze P, Nørskov JK. 1995. *Phys. Rev. Lett.* 74: 2295
84. Schwoebel RL, Shipsey EJ. 1966. *J. Appl. Phys.* 37:3682
84a. Ehrlich G, Hudda FG. 1966. *J. Chem. Phys.* 44:1039
85. Gölzhäser A, Ehrlich G. 1996. *Phys. Rev. Lett.* 77:1334
86. Nørskov JK, Jacobsen KW, Stoltze P, Hansen LB. 1993. *Surf. Sci.* 283:277
87. Wang SC, Ehrlich G. 1991. *Phys. Rev. Lett.* 67:2509
88. Li Y, DePristo AE. 1996. *Surf. Sci.* 319:141
88a. Li Y, DePristo AE. 1996. *Surf. Sci.* 351:189
89. Siswanto G, Jónsson H, (to be published).
90. Kellogg GL, Voter AF. 1991. *Phys. Rev. Lett.* 67:622
90a. Liu S, Zhang Z, Nørskov JK, Metiu H. 1994. *Surf. Sci.* 321:161
90b. Liu S, Zhang Z, Comsa G, Metiu H. 1993. *Phys. Rev. Lett.* 71:2967
90c. Liu S, Metiu H. 1996. *Surf. Sci.* 359: 245
90d. Li Y, Raeker TJ, DePristo AE. 1994. *Phys. Rev. B* 50:14742
91. Langer JS. 1986. In *Direction in Condensed Matter Physics*, pp. 165–86 Singapore: World Sci.
91a. Langer JS. 1987. In *Chance & Matter, Les Houches Summer School Lect. Sess.*, 46, ed. J Souletie, J Vannimenus, R. Stora, p. 629. Amsterdam: Elsevier
92. Cahn JW, Hilliard JE. 1958. *J. Chem. Phys.* 28:259
93. McFadden GB, Wheeler AA, Braun RJ, Coriell SR, Sekerka RF. 1993. *Phys. Rev. E* 48:2016
94. Penrose O, Fife PC. 1990. *Phys. D* 43: 44
95. Berne BJ, Ciccotti G, Coker DF, eds. 1998. *Classical and Quantum Dynamics in Condensed Phase Stimulations*. Singapore: World Sci.

Annual Review of Physical Chemistry
Volume 51, 2000

CONTENTS

Fifty Years in Physical Chemistry: Homage to Mentors, Methods, and Molecules, *Dudley Herschbach* 1

SURFACE PLASMON RESONANCE IMAGING MEASUREMENTS OF ULTRATHIN ORGANIC FILMS, *Jennifer M. Brockman, Bryce P. Nelson, Robert M. Corn* 41

Delayed Ionization and Fragmentation En Route to Thermionic Emission: Statistics and Dynamics, *E. E. B. Campbell, R. D. Levine* 65

Spatially Heterogeneous Dynamics in Supercooled Liquids, *M. D. Ediger* 99

Generalized Born Models of Macromolecular Solvation Effects, *Donald Bashford, David A. Case* 129

Chemical Dynamics at Metal Surfaces, *John C. Tully* 153

Peptides and Proteins in the Vapor Phase, *Martin F. Jarrold* 179

Effective Interactions Between Electric Double Layers, *Jean-Pierre Hansen, Hartmut Löwen* 209

Transient Lasar Frequency Modulation Spectroscopy , *Jean-Pierre Hansen, Hartmut Löwen* 243

Motion and Disorder in Crystal Structure Analysis: Measuring and Distinguishing Them, *H. B. Bürgi* 275

Quantitative Atom-Atom Potentials from Rotational Tunneling: Their Extraction and Their Use, *M. R. Johnson, G. J. Kearley* 297

Decoding the Dynamical Information Embedded in Highly Mixed Quantum States, *John C. Keske, Brooks H. Pate* 323

Large-Scale Shape Changes in Proteins and Macromolecular Complexes, *Michael E. Wall, Stephen C. Gallagher, Jill Trewhella* 355

Reflection Absorption Infrared Spectroscopy and the Structure of Molecular Adsorbates on Metal Surfaces, *Michael Trenary* 381

The Dynamics of Noble Gas-Halogen Molecules and Clusters, *Andreas Rohrbacher, Nadine Halberstadt, Kenneth C. Janda* 405

Molecular Dynamics Simulation of Nucleic Acids, *Thomas E. Cheatham III, Peter A. Kollman* 435

Chemistry and Microphysics of Polar Stratospheric Clouds and Cirrus Clouds, *Mark A. Zondlo, Paula K. Hudson, Anthony J. Prenni, Margaret A. Tolbert* 473

Monte Carlo Methods in Electronic Structures for Large Systems, *Arne Lüchow, James B. Anderson* 501

Thermodynamics of the Size and Shape of Nanocrystals: Epitaxial Ge on Si(001), *R. Stanley Williams, Gilberto Medeiros-Ribeiro, Theodore I. Kamins, Douglas A. A. Ohlberg* 527

Semiclassical Calculation of Chemical Reaction Dynamics via Wavepacket Correlation Functions, *David J. Tannor, Sophya Garashchuk* 553

Self-Assembled Ceramics Produced by Complex-Fluid Templation, *Daniel M. Dabbs, Ilhan A. Aksay* 601

Theoretical Studies of Atomic-Scale Processes Relevant to Crystal Growth, *Hannes Jónsson* 623

New Technologies in Electron Spin Resonance, *Jack H. Freed* 655

Multidimensional Femtosecond Correlation Spectroscopies of Electronic and Vibrational Excitations, *Shaul Mukamel* 691

Structures and Dynamics of Molecules on Liquid Beam Surfaces, *Tamotsu Kondow, Fumitaka Mafuné* 731
Effects of High Pressure on Molecules, *Russell J. Hemley* 763